Journal of Sound and Vibration (1998) **213**(2), 235–257

AFT FAN DUCT ACOUSTIC RADIATION

W. EVERSMAN

Department of Mechanical and Aerospace Engineering and Engineering Mechanics, University of Missouri-Rolla, Rolla, MO 65401, *U.S.A.*

AND

D. OKUNBOR

Department of Computer Science, University of Missouri-Rolla, Rolla, MO 65401, *U.S.A.*

(*Received* 13 *June* 1997, *and in final form* 18 *December* 1997)

A finite element code has been developed for the prediction of the radiated acoustic field from the aft fan duct of a turbofan engine. The acoustic field is modelled based on the assumption that the steady flow in and around the nacelle is irrotational as is the acoustic perturbation. The geometry of the nacelle is axisymmetric and the acoustic source is harmonic and decomposed into its angular harmonics. The steady flow is computed on the acoustic mesh and provides data for the acoustic calculations. The jet is included in the steady flow potential flow model by separating the interior and exterior flow outside the aft fan duct with a thin barrier created by disconnecting the computational domain. The jet and exterior flow are allowed to merge at a defined distance downstream. In the acoustic radiation model continuity of acoustic particle velocity is implicitly satisfied across the shear layer by careful treatment of the surface integral which appears in the finite element method (FEM) formulation. Pressure continuity is enforced by using a penalty constraint on the shear layer. A model for locally reacting acoustic treatment provides a boundary condition on the duct walls. An attempt has been made to limit reflections on the artificial baffle introduced to limit the computational domain, but this is only moderately successful. An old, but reliable frontal solution routine has been updated with considerable impact on computational time. Example calculations are given which show the success achieved in satisfying the complicated interface conditions on the shear layer and the characteristics of the solutions at relatively high frequencies where the refinement of the mesh becomes a limiting consideration for practical computations.

1. INTRODUCTION

In approach and cutback conditions the acoustic field from high by-pass ratio turbofan engines is dominated by tonal noise generated by blade/vane interactions and radiated forward from the nacelle inlet and to the rear from the aft fan duct. In order to meet noise control goals active and passive techniques can be employed to control the source mechanisms and to attenuate acoustic propagation in the inlet and fan exhaust ducts. Methods for the prediction of the effects of various noise control measures on far field acoustic radiation are required in the design process. The investigation reported here is directed toward the development of a robust computational scheme for the prediction of the acoustic field attributed to tonal sources typical of blade/vane interaction in the aft fan duct. It is intended to be coupled to a suitable model of the source mechanism.

The model developed is an extension of computational methods which were developed for inlet radiation [1–4]. The inlet radiation model was based on the assumption of

0022–460X/98/220235 + 23 $25.00/0/sv971480

irrotational acoustic perturbations on an irrotational steady flow. A finite element code was developed which could accurately model the geometric details of an axisymmetric inlet as well as the steady flow field in and around the inlet, including the effect of forward flight. Rapid advances in the capabilities of work stations has made it a realistic goal to accurately predict the acoustic field around realistic geometries at realistic frequencies. Reported here is the development of a similar model for aft radiated noise. The most significant extension is the representation of the important effects of the fan duct jet imbedded in the surrounding flow which includes forward flight effects. The presence of the jet introduces interesting conditions which must be imposed on acoustic propagation across the shear layer which confines it. The methods for achieving these conditions in the context of the finite element method (FEM) are discussed in detail here.

2. FORMULATION OF THE ACOUSTIC RADIATION PROBLEM

The aft radiated acoustic field from a turbofan nacelle is described by a potential formulation as previously introduced for inlet acoustic radiation [1–4]. Figure 1 is a sketch of the important geometrical features of the aft fan duct and centre body. The nacelle has a forward flight Mach number M_0, which at large distances is equivalent to a uniform flow directed away from the fan exhaust duct exit plane. Near the nacelle this velocity field is non-uniform. The exhaust flow, defined at the source plane by Mach number M_j, emerges as a potential flow jet and extends down stream confined by a shear layer separating it from the exterior flow. The shear layer is terminated at a defined length at which point the jet and external flow merge as potential flows. The potential flow merging of the jet and exterior flow at the end of the shear layer produces a localized steady flow anomaly which has not been observed to substantially influence the acoustic radiation. Computations are to be carried out using the FEM in a domain including the interior of the aft fan exhaust duct and an exterior region made finite by invoking a radiation condition at an outer computational boundary and by introducing an artificial baffle oriented to produce a minimal effect on the acoustic radiation field.

The nacelle geometry and the steady flow field are assumed to be axially symmetric. The noise source is assumed to be harmonic in time and is decomposed into its angular modal content, allowing a two-dimensional representation of the acoustic field in an (x, r) plane through the nacelle axis of symmetry. The solution domain is shown in Figure 2. It is the x, r plane in cylindrical co-ordinates. The source plane is designated by C_f. The fan or exit guide vane source is input on this plane by specifying complex amplitudes of incident duct modes (see references [1–4] for details of the implementation of the source boundary

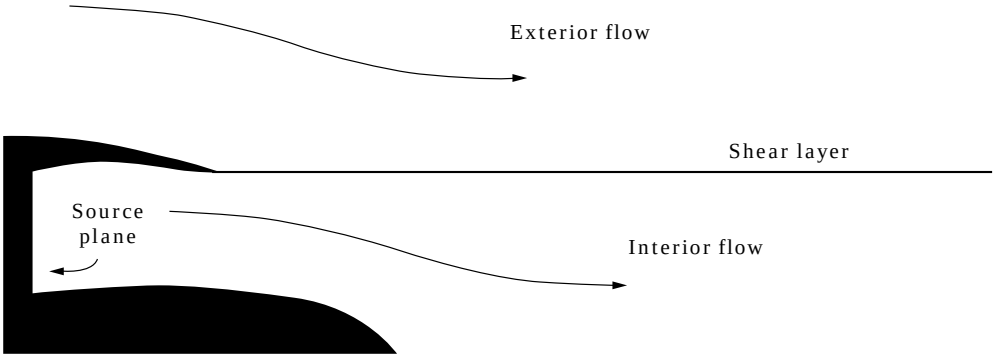

Figure 1. Sketch of the geometry of the aft fan duct, emphasizing the exhaust flow and shear layer.

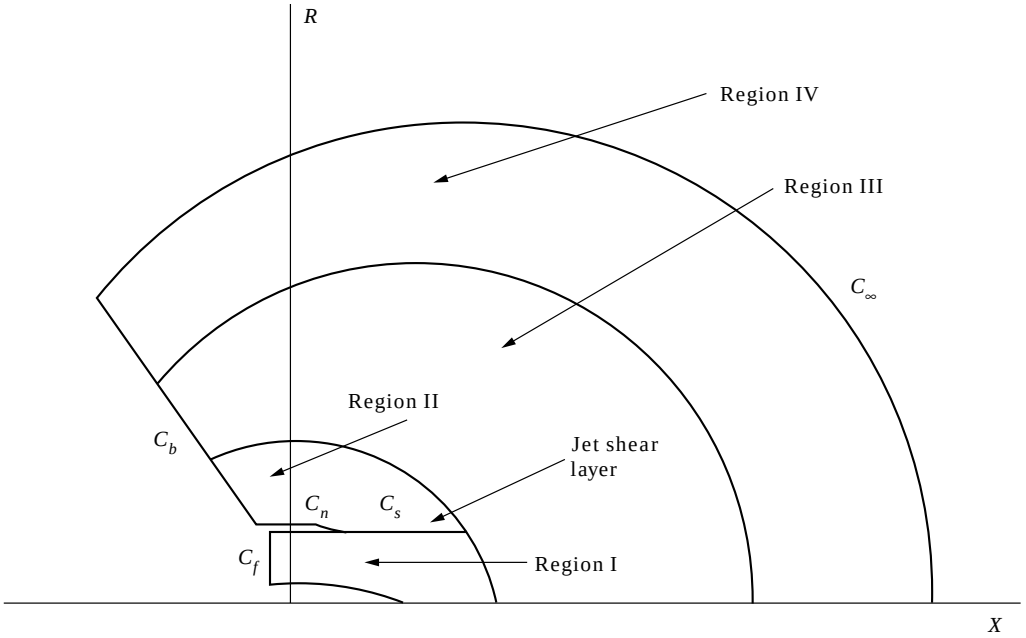

Figure 2. Computational domain showing the boundaries and regions.

condition.). The nacelle outer surface is C_n. The outer boundary of the solution domain C_∞ is a circle which is a constant phase surface for an acoustic source located at the origin. On this boundary a radiation condition is specified. Wave envelope elements [1–4] are used in the far field to reach the outer boundary with minimal cost in mesh refinement. An artificial baffle C_b limits the solution domain well upstream of the fan exit plane and is chosen to be swept in such a way that a minimal effect on the acoustic field is created. This baffle is a ray from the origin and in principle at large distances from the source it should be non-reflecting, although near field effects do lead to reflection. The placement of the baffle must be considered in terms of the likely orientation of the radiated field. The baffle can be eliminated if computational efficiency is not a limiting factor. The shear layer C_s which separates the potential flow jet from the potential exterior flow is a rigid boundary for the calculation of the steady flow field and is a surface across which appropriate continuity conditions must be satisfied in the acoustic calculations.

The starting point for the formulation of both the steady mean flow and the acoustic perturbation consists of the mass and momentum equations and the energy equation in the form of the isentropic equation of state:

$$\frac{\partial \hat{\rho}}{\partial t} + \nabla \cdot (\hat{\rho}\mathbf{V}) = 0, \tag{1}$$

$$\frac{\partial \mathbf{V}}{\partial t} + (\mathbf{V} \cdot \nabla)\mathbf{V} = -\frac{1}{\hat{\rho}} \nabla \hat{p}, \qquad \frac{\hat{p}}{p_0} = \left(\frac{\hat{\rho}}{\rho_0}\right)^\gamma, \tag{2, 3}$$

where $\hat{p}$, $\hat{\rho}$ and $\mathbf{V}$ are fluid properties pressure, density and velocity, at this point in dimensional form, and p_0 and ρ_0 are reference values of pressure and density.

A weak form of the field equations begins with equation (1) in which solutions for $\hat{\rho}$ and $\mathbf{V}$ are sought in the class of continuous functions which satisfy the weighted residual relation

$$\iiint_V \left[\nabla W \cdot (\hat{\rho}\mathbf{V}) - W \frac{\partial \hat{\rho}}{\partial t} \right] \mathrm{d}V = \iint_S W \hat{\rho} \mathbf{V} \cdot \mathbf{n} \, \mathrm{d}S \tag{4}$$

for every function $W(\mathbf{x})$ in the class of continuous functions. The surface integral is over the boundaries of the domain of solution and $\mathbf{n}$ is the unit normal out of the domain. In the finite element discretization process which follows, the surface integral must also be interpreted at each subdomain boundary, namely the boundaries of the individual elements. The physical boundaries of the solution domain include the boundaries of the nacelle, including the source plane, the rigid structural boundaries, and absorbing boundaries such as acoustic treatment. Other boundaries are the artificial baffle introduced to limit the solution domain and the outer boundary of the solution domain at which a radiation condition is applied. All of these boundary conditions are introduced through the surface integral. The boundary integral is observed to involve the mass flux normal to the boundary. The integral is therefore in terms of an essential conservation quantity, and this is typical of weak formulations in the framework of the FEM. For boundaries between subdomains (elements) in the FEM discretization at which there is no surface of discontinuity the integral produces no net contribution. This follows because on such boundaries the integrals on either side of the boundary produce contributions equal in magnitude and opposite in sign. In the present problem this applies to all boundaries between elements, although, as will be shown, a careful interpretation of the surface integral must be carried out to establish that it vanishes across the shear layer separating the outer flow field from the jet with a discontinuity in tangential steady flow. In particular, it seems to be necessary to start from the yet to be linearized form of the weighted continuity equation (1), and to carefully linearize it to account for the fact that on the shear layer, which is displaced due to acoustic perturbations, the integral is interpreted to be evaluated on the surface of discontinuity in tangential steady flow velocity with the unit normal defined to reflect this. If the field equation is linearized before the weak formulation is established, an essential contribution to the boundary integral is lost.

3. BOUNDARY CONDITIONS ON THE SHEAR LAYER

Figure 3 shows the idealized interface between the exterior flow and the jet. The surface of discontinuity in tangential velocity is assumed to be displaced from the mean position by

$$\Delta r(x, \theta, t) = \zeta(x, \theta, t), \tag{5}$$

where $\zeta(x, \theta, t)$ is an acoustic perturbation. The normal to the interface is tilted due to the slope of the shear layer approximately by

$$\Delta \mathbf{n}_b = -\frac{\partial \zeta}{\partial x} \mathbf{n}_t, \tag{6}$$

where $\mathbf{n}_b$ can be written in terms of the unit vectors $\mathbf{n}$, $\mathbf{n}_t$, which are normal and tangent to the undisplaced shear layer, in the form

$$\mathbf{n}_b = \mathbf{n} - \frac{\partial \zeta}{\partial x} \mathbf{n}_t. \tag{7}$$

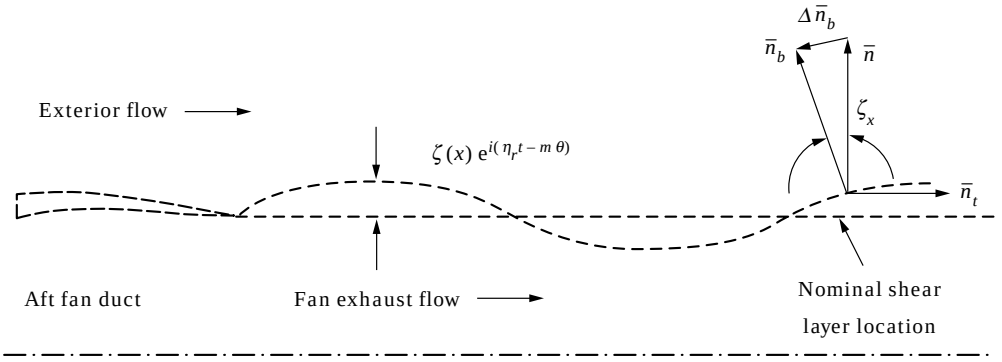

Figure 3. Geometry of the shear layer interface, showing the acoustically displaced boundary between the jet and exterior flow.

The orientation of the unit normals here are consistent with the surface below the shear layer for which the normal out of the fluid is in the direction of the positive normal fluid particle velocity, but a similar argument applies if the surface above the shear layer is considered. The tangential component of the normal to the shear layer is an acoustic perturbation quantity.

The interface conditions across the shear layer can be determined by examining the mass flux and momentum flux at a moving surface of discontinuity. A particularly good explanation is given by Karamcheti [5]. The essential results in the case of a discontinuity in the velocity tangential to the surface of discontinuity are:

$$(\mathbf{V}_u - \mathbf{V}_s)\cdot\mathbf{n}_b = (\mathbf{V}_l - \mathbf{V}_s)\cdot\mathbf{n}_b = 0, \qquad \hat{\rho}_u(\mathbf{V}_u - \mathbf{V}_s)\cdot\mathbf{n}_b - \hat{\rho}_l(\mathbf{V}_l - \mathbf{V}_s)\cdot\mathbf{n}_b = 0, \quad (8, 9)$$

$$\hat{\rho}_u\mathbf{V}_u\cdot\mathbf{n}_b(\mathbf{V}_u - \mathbf{V}_s)\cdot\mathbf{n}_b - \hat{\rho}_l\mathbf{V}_l\cdot\mathbf{n}_b(\mathbf{V}_l - \mathbf{V}_s)\cdot\mathbf{n}_b = \hat{p}_l - \hat{p}_u. \quad (10)$$

Here $\mathbf{V}_u$ and $\mathbf{V}_l$ are the fluid velocity above and below the discontinuity and $\mathbf{V}_s$ is the velocity of an element on the surface of discontinuity. $\hat{\rho}_u$ and $\hat{\rho}_l$ are the fluid densities above and below the discontinuity and $\hat{p}_u$ and $\hat{p}_l$ are the corresponding pressures. Equation (8) follows from the tangential component of the momentum equation and equation (9) from the mass continuity equation. Equation (9) is satisfied automatically due to equation (8). Equation (10) is the component of the momentum equation normal to the discontinuity. With equations (8) and (10) it is determined that

$$\hat{p}_u = \hat{p}_l, \quad (11)$$

which is the condition that pressure be continuous across the shear layer. The linearized version of this would require the acoustic perturbation in pressure to be continuous as well as the pressure of the steady flow.

A linearized version of the surface integral of equation (4) is required for the acoustic analysis which follows. The fluid velocities are replaced by their perturbation forms $\mathbf{V}_u = V_{r_u}\mathbf{n}_t + \mathbf{v}_u$ and $\mathbf{V}_l = V_{r_l}\mathbf{n}_t + \mathbf{v}_l$, where V_{r_u} and V_{r_l} are the mean flow tangential velocities above and below the discontinuity. The densities are replaced by $\hat{\rho}_u = \rho_{r_u} + \rho_u$ and $\hat{\rho}_l = \rho_{r_l} + \rho_l$ with the possibly different mean densities given by ρ_{r_u} and ρ_{r_l}. The acoustic quantities are now ρ_u and ρ_l. It is also important to note that the velocity of an element of the surface of discontinuity is an acoustic quantity and is therefore denoted by $\mathbf{V}_s = \mathbf{v}_s$.

Equation (7), and equation (8) in linearized form, are equivalent to the familiar conditions of continuity of particle displacement,

$$\mathbf{v}_u \cdot \mathbf{n} = \frac{\partial \zeta}{\partial t} + V_{r_u} \frac{\partial \zeta}{\partial x}, \qquad \mathbf{v}_l \cdot \mathbf{n} = \frac{\partial \zeta}{\partial t} + V_{r_l} \frac{\partial \zeta}{\partial x}. \tag{12, 13}$$

The linearized form of the surface integral of equation (4) on the upper and lower surfaces of the shear layer can then be obtained by using equation (7) and equations (12) and (13) (and accounting properly for the evaluation of the integral on the surface above the shear layer):

$$\iint_{S_{s_l}} W(\hat{\rho}\mathbf{V})_l \cdot \mathbf{n}_{b_l} \, \mathrm{d}S = \iint_{S_{s_l}} W \rho_{r_l} \frac{\partial \zeta}{\partial t} \, \mathrm{d}S, \tag{14}$$

$$\iint_{S_{s_u}} W(\hat{\rho}\mathbf{V})_u \cdot \mathbf{n}_{b_u} \, \mathrm{d}S = -\iint_{S_{s_u}} W \rho_{r_u} \frac{\partial \zeta}{\partial t} \, \mathrm{d}S. \tag{15}$$

It is apparent from equations (14) and (15) that along the shear layer the net contribution of the surface integrals will vanish if the steady flow densities above and below the shear layer are the same. If they are different, as in the case of a hot jet in a cold outer medium, there will be a net contribution which is effectively a distributed source on the shear layer with a strength proportional to the difference in the steady flow densities. This is completely consistent with equation (9). It is also consistent with the rigorous analysis given by Myers [6].

4. LINEARIZED WEAK FORMULATION

A linearized weak formulation is obtained by continuing with equation (4) for which the linearization of the boundary integral has been examined. Acoustic propagation and radiation is modelled based on the assumption that the mean flow in and around the nacelle is irrotational and that the acoustic perturbation is also irrotational. The potential formulation makes it possible to introduce mean flow and acoustic perturbation velocity potentials. Acoustic perturbations are assumed on the steady mean flow such that $\hat{\phi} = \phi_r + \phi$, $\hat{\rho} = \rho_r + \rho$ and $\hat{p} = p_r + p$. The acoustic perturbations are assumed to be harmonic in time and in the angular co-ordinate such that $\rho(x, r, \theta, t) = \rho(x, r)\, \mathrm{e}^{\mathrm{i}(\eta_r t - m\theta)}$, $p(x, r, \theta, t) = p(x, r)\, \mathrm{e}^{\mathrm{i}(\eta_r t - m\theta)}$ and $\phi(x, r, \theta, t) = \phi(x, r)\, \mathrm{e}^{\mathrm{i}(\eta_r t - m\theta)}$. The acoustic perturbation in the shear layer position is also assumed to be harmonic in time and the angular co-ordinate yielding $\zeta(x, \theta, t) = \zeta(x)\, \mathrm{e}^{\mathrm{i}(\eta_r t - m\theta)}$. The steady flow density and velocity are ρ_r, $\nabla\phi_r$. In linearized form, the weak formulation of equation (4) becomes [4]

$$\iiint_V \{\nabla W \cdot (\rho_r \nabla\phi + \rho \nabla\phi_r) - \mathrm{i}\eta_r W \rho\} \, \mathrm{d}V = \mathrm{i}\eta_r \iint_{S_s} W(\rho_{r_l} - \rho_{r_u})\zeta \, \mathrm{d}S + \iint_S W(\rho_r \nabla\phi + \rho\nabla\phi_r) \cdot \mathbf{n} \, \mathrm{d}S. \tag{16}$$

The weighting functions are taken as $W(x, r, \theta) = W(x, r)\, \mathrm{e}^{\mathrm{i}m\theta}$. Perturbations are in the form of angular harmonics proportional to $\mathrm{e}^{-\mathrm{i}m\theta}$ representing the decomposition of the

solution periodic in θ in a Fourier Series. The angular mode number is a parameter of the solution. The first surface integral on the right hand side is on the shear layer S_s and the second surface integral is over all remaining surfaces bounding the domain. Notice that the unit normal for the second integral is the normal out of the domain at the surface in question. The weak formulation continues with the linearized momentum equation [4]

$$\rho = -\frac{\rho_r}{c_r^2}(\mathrm{i}\eta_r\phi + \nabla\phi_r \cdot \nabla\phi), \tag{17}$$

which is used to replace ρ in equation (16), the linearized equation of state,

$$p = c_r^2\rho, \tag{18}$$

which is used to produce an alternative form of the momentum equation in terms of acoustic pressure,

$$p = -\rho_r(\mathrm{i}\eta_r\phi + \nabla\phi_r \cdot \nabla\phi). \tag{19}$$

Equation (19) is used to define acoustic pressure difference on the shear layer and to post-process the field solution for ϕ to obtain the acoustic pressure field. The acoustic particle velocity and acoustic velocity potential are related according to

$$\mathbf{v} = \nabla\phi. \tag{20}$$

The linearization process also produces the weighted residual formulation for the steady flow,

$$\iiint_V \nabla W \cdot (\rho_r \nabla\phi_r)\,\mathrm{d}V = \iint_S W(\rho_r\nabla\phi_r)\cdot\mathbf{n}\,\mathrm{d}S, \tag{21}$$

and the steady flow momentum equation in terms of the speed of sound,

$$c_r^2 = 1 - \frac{(\gamma-1)}{2}[\nabla\phi_r\cdot\nabla\phi_r - M_\infty^2], \tag{22}$$

and in terms of the steady flow density,

$$\rho_r = \left[1 - \frac{(\gamma-1)}{2}(\nabla\phi_r\cdot\nabla\phi_r - M_\infty^2)\right]^{1/(\gamma-1)}. \tag{23}$$

Equations (16) through (23) are in non-dimensional form where ϕ is the acoustic potential, ϕ_r is the local mean flow (reference) potential, ρ is the acoustic density, ρ_r is the local mean flow density, and c_r is the local speed of sound in the mean flow. All quantities are made non-dimensional by using the density in the far field, ρ_∞, the speed of sound in the far field, c_∞, and a reference length which is defined as the duct radius at the source plane, R, where acoustic modal amplitudes are defined. This plane could be the fan plane or the exit guide vane plane, but it is not restricted to these locations. The acoustic potential is non-dimensional with respect to $c_\infty R$, and the acoustic pressure with respect to $\rho_\infty c_\infty^2$. Lengths are made non-dimensional with respect to R. Time is scaled with R/c_∞, leading to the definition of non-dimensional frequency $\eta_r = \omega R/c_\infty$; ω is the dimensional source frequency and $M_\infty = M_o$ is the Mach number in the far field representing the forward flight effect.

Equation (21) is the weighted residual formulation for the calculation of the compressible potential flow within and around the nacelle. Equations (22) and (23) are subsidiary relations that can be used in an iterative solution which at each stage uses a density field derived from the previous iteration step. $\nabla\phi_r$, c_r, ρ_r are required data for the weighted residual formulation of the acoustic problem. In the results reported here only the first iteration of this process is used to define the potential flow field. This is accomplished by solving the incompressible problem and then computing a variation in steady flow density and speed of sound.

The second surface integral in equation (16) provides the boundary conditions on the duct walls and on the source plane. The modelling of duct acoustic treatment in the context of this integral is discussed in a later section. The acoustic source is specified by the complex amplitudes of acoustic duct modes at the source plane. On this plane the FEM modal values of acoustic potential are replaced by the complex amplitudes of the acoustic potential modes by an eigenfunction expansion. The incident acoustic modal amplitudes are input and the reflected modal amplitudes are computed as part of the solution. Details of this procedure are available in references [1–4].

The same surface integral provides the mechanism for introducing the boundary conditions on the artificial baffle and the non-reflecting boundary condition at large distances on the outer boundary of the computational domain. These details are also explained extensively in references [1–4].

Acoustic pressure and particle displacement are continuous across the shear layer. The continuity of particle displacement is implicit in the handling of the surface integral on the shear layer. Continuity of pressure must be explicitly enforced. The implementation of this condition will be discussed presently.

5. COMPUTATIONAL MESH

A particularly sensitive issue which must be resolved is the construction of a mesh which is consistent with the geometry requirements and which can be generated automatically from data describing the nacelle and centre body. It is essential that the mesh be structured to minimize the bandwidth for the linear equation solver. The major constraining feature is that the trailing edge of the fan duct is thin or cusped. In addition, the near field mesh must evolve into a smooth transition to the far field wave envelope mesh.

In order to meet all of these requirements, a mesh which combines quadrilateral and triangular elements has been used. Figure 4 shows the details of the near field mesh. The interior of the duct and the extended jet uses conventional eight-node quadrilateral elements. Most of the exterior region is also composed of quadrilateral elements. However, a fan shaped region of six-node triangular elements is used to allow a transition around the sharp trialing edge. Primarily due to the constraint on the mesh structure for minimizing bandwidth, this transition would not be possible with rectangular elements without introducing severe distortion in the neighbourhood of the trailing edge. The far field mesh utilizes the wave envelope element concept [1–4], and presents no problems. A relatively coarse near and far field mesh is shown in Figure 5 and the wave envelope element region can be seen. Note in Figure 4 that the exhaust duct trailing edge is reflexed, representing the most severe case.

Mesh generation produces two mesh connectivities. For the potential flow code, velocity potential is discontinuous across the shear layer dividing the extended jet from the external flow. Elements are therefore disconnected across the shear layer. For the radiation code, acoustic velocity potential is also discontinuous across the shear layer. Elements above and below the shear layer have additional degrees of freedom on the shear layer boundaries

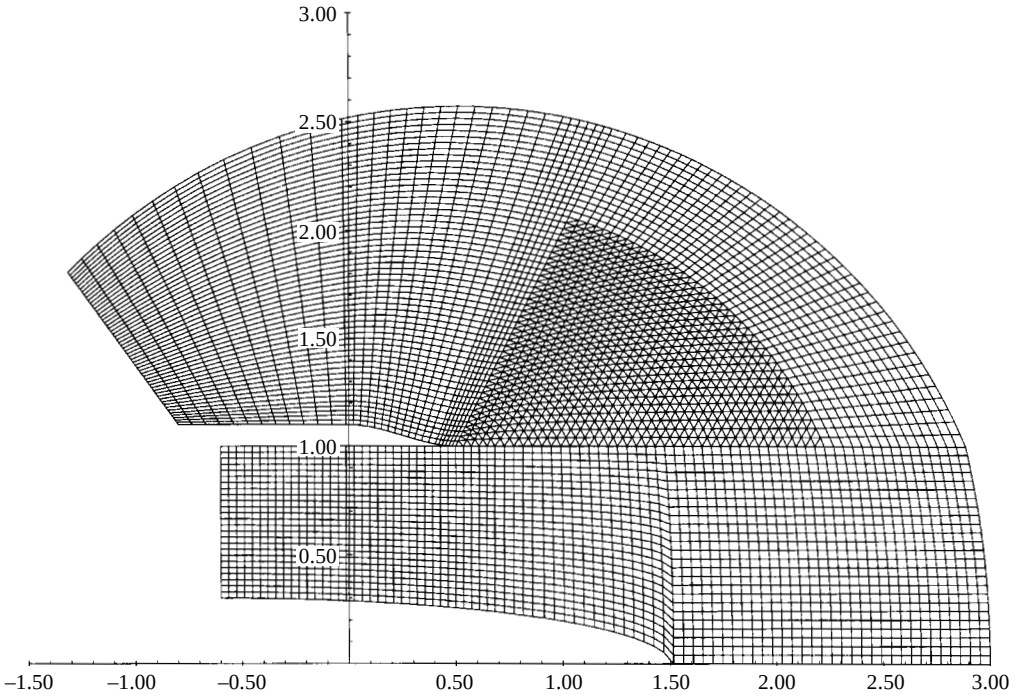

Figure 4. Aft fan duct near field mesh.

representing acoustic particle displacement, which is continuous across the shear layer. The mesh for the radiation code therefore introduces two degrees of freedom at the nodes on the shear layer. There are 11 degrees of freedom for rectangular elements and nine degrees of freedom for triangular elements on the shear layer. Pressure continuity is enforced by

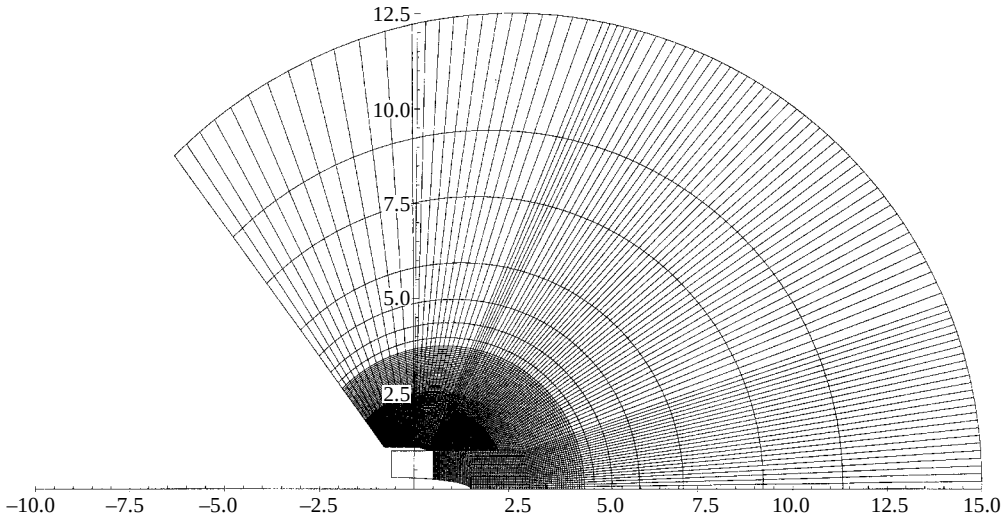

Figure 5. Aft fan duct far field mesh with wave envelope region.

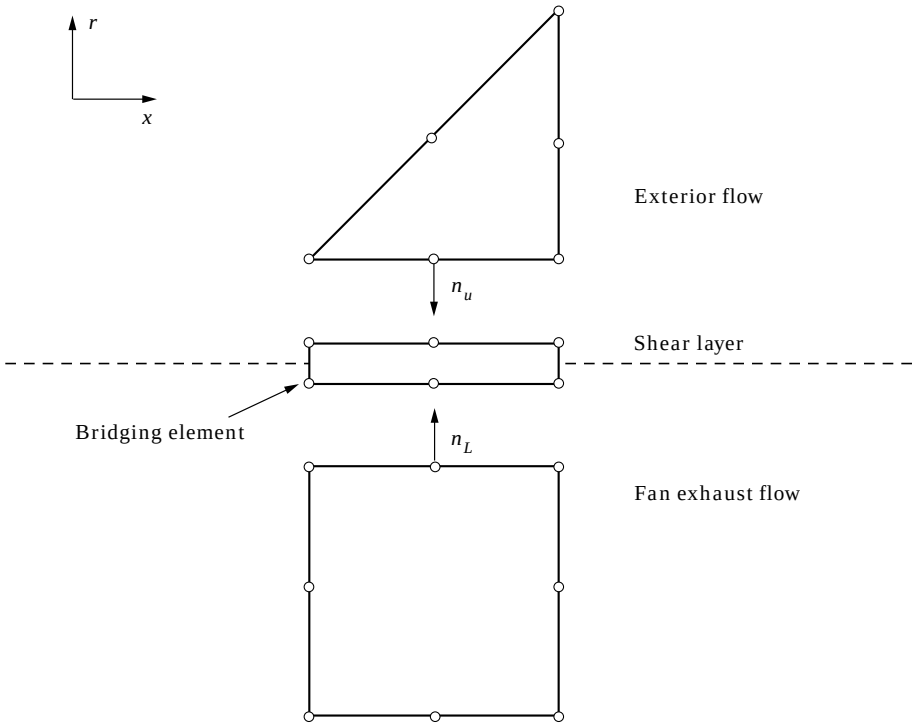

Figure 6. Bridging elements on the shear layer.

using a penalty constraint on the shear layer, and it is not necessary to introduce pressure as an additional variable on the shear layer. However, it has been found convenient to introduce six-node "rectangular" transition elements of zero thickness between the standard elements above and below the shear layer for generating the "penalty element stiffness matrices". In order to maintain consistency in the meshes for the potential flow calculations and radiation calculations, these elements are accounted for in mesh generation for both codes. Details of the elements on the shear layer are shown in Figure 6 where for an example a bridging element is inserted between a triangular element above the shear layer and a rectangular element below the shear layer.

6. STEADY FLOW CALCULATIONS

A potential flow code generates the steady flow field in and around the aft fan duct. Incompressible potential flow has been assumed as a first approximation. Variations in density and speed of sound are based on the isentropic equation of state and incompressible velocity field with specified conditions on Mach number, density, and speed of sound in the far field. It is within the framework of the general formulation to treat the potential mean flow as compressible, and the present approach can be viewed as the "zeroth" iteration of the compressible isentropic case. Fully compressible isentropic mean flow has been used by the first author in acoustic propagation and scattering calculations in pipes in which no far field radiation is modelled. In the type of problem considered here the computational overhead required for the several iterations necessary to produce a compressible mean flow has not been considered justifiable at the present stage of development.

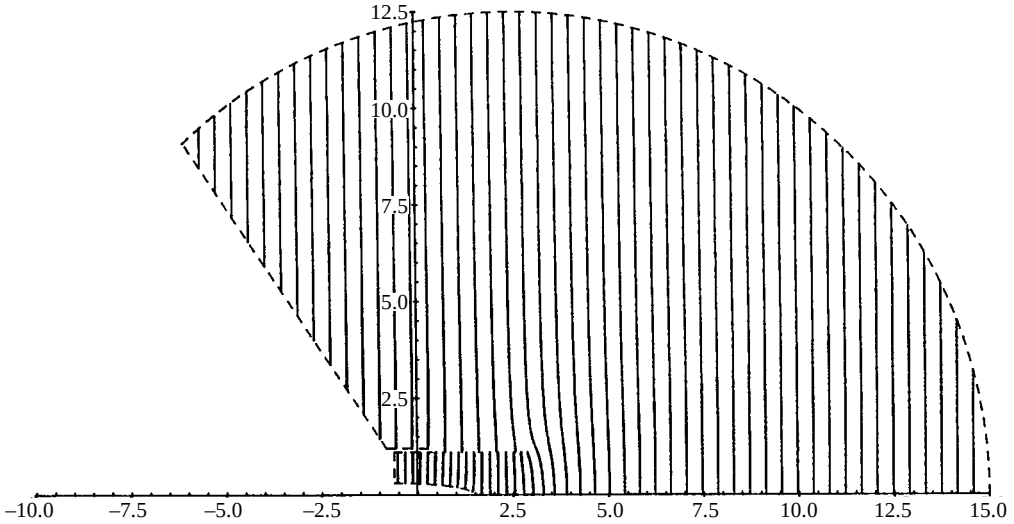

Figure 7. Potential field for the steady flow from the aft fan duct and in the surrounding flow field. This case corresponds to $M_j = 0{\cdot}5$ and forward flight velocity $M_0 = 0{\cdot}2$.

The potential flow field has been structured to include flow in a jet region downstream of the fan duct exit plane. This has been done with the introduction of a "rigid" duct boundary representing the fan exhaust shear layer which extends the prescribed length of the jet. The rigid boundary is introduced by permitting the velocity potential to be discontinuous across the shear layer. At the downstream end of the shear layer the discontinuity in velocity potential is terminated and merging of the interior and external flows is permitted. The merging can produce very high velocities and reverse flow near the termination of the shear layer. This is smoothed out by restricting the velocity near the end of the shear layer to neither go above a reference velocity which is determined midway along the underside of the shear layer (in the jet) nor to go below a similarly determined velocity on the upper side of the shear layer (in the outer flow). In the near field mesh of Figure 4 the shear layer boundary can be seen to extend downstream about two duct radii. The merging distance is adjustable, and is chosen to provide sufficient distance for full effect on the acoustic radiation, and to move the perhaps unrealistic merging region away from the important part of the acoustic field. Computations for the steady flow field are carried out on the same mesh used in the acoustic case. This is done so that the steady flow data is produced in a form compatible with the acoustic mesh. The mesh is invariably much more dense than would be required for the steady flow calculations, however, the problem is symmetric, and the solution routine is considerably faster than for the comparable acoustic problem (about three or four times faster for large meshes).

A typical potential flow field is shown in Figure 7, where the jet and surrounding forward flight effect contours of velocity potential are clearly shown.

7. ACOUSTIC PRESSURE CONTINUITY ON THE SHEAR LAYER

The linearized weak formulation of equation (16) has the subsidiary condition of continuity of acoustic pressure across the shear layer. This condition is not easily satisfied because the formulation is in terms of acoustic velocity potential. However, equation (19) provides a connection between the acoustic velocity potential above and below the shear

layer which can be exploited to implement the continuity condition by using a penalty method [7].

The important features of the penalty method can be described relatively easily. Equation (19) and the condition pressure continuity on the shear layer are used to obtain

$$\Delta p = p_u - p_l = \rho_{r_l}\left(\mathrm{i}\eta_r\phi_l + M_l\frac{\partial\phi_l}{\partial x}\right) - \rho_{r_u}\left(\mathrm{i}\eta_r\phi_u + M_u\frac{\partial\phi_u}{\partial x}\right) = 0. \tag{24}$$

Equation (24) applies computationally on the shear layer, $r = r_j$, $x_1 \leqslant x \leqslant x_2$, where r_j is the radius of the axially symmetric shear layer and x_1, x_2 are the axial co-ordinates of the left and right ends of the shear layer; x_1 coincides with the trailing edge of the nacelle at the fan exit plane. The subscripts l and u denote values of the steady state and acoustic quantities below and above the shear layer. In the finite element context, the acoustic potentials ϕ_l and ϕ_u can be written notionally in terms of a global interpolation matrix $[N(x)]$. For example,

$$\phi_l(x) = [N(x)]\underline{\phi}_l, \tag{25}$$

where $\underline{\phi}_l$ is the vector of nodal values of $\phi_l(x)$ below the shear layer. The interpolation matrix $[N(x)]$ is a row matrix with elements $N_i(x)$, $i = 1, NN$, where NN is the number of finite element nodes and $N_i(x_j) = 1$, $i = j$, $N_i(x_j) = 0$, $i \neq j$, $j = 1, NN$. The substantial derivative operators in equation (24) are defined such that, for example,

$$D_l(\phi_l) = \rho_{r_l}\left(\mathrm{i}\eta_r + M_l\frac{\partial}{\partial x}\right)\phi_l. \tag{26}$$

In vector–matrix format,

$$D_l(\phi_l) = [N(x)][D_l]\underline{\phi}_l, \tag{27}$$

where $[D_l]$ is a diagonal matrix of operators $\rho_{r_l}(\mathrm{i}\eta_r + M_l\,\partial/\partial x)$. Equation (24) can be written as

$$[N_p(x)][\phi_l, \phi_u]^T = ([N(x)][D_l] - [N(x)][D_u])[\phi_l, \phi_u]^T = 0. \tag{28}$$

The modified interpolation matrix $[N_p(x)]$ has elements which can be viewed as interpolating $\Delta p(x)$ from nodal values of the acoustic potential on either side of the shear layer. The weighted residual of equation (28) is formed on the shear layer using as weighting functions elements of $[N_p^*(x)]$, which are the complex conjugates of the interpolation functions. This yields

$$\iint_{S_s} [N_p^*(x)]^T[N_p(x)]\,\mathrm{d}S_s[\phi_l, \phi_u]^T = 0. \tag{29}$$

This is a weighted residual (or variational) statement that Δp vanishes on the shear layer. It produces a "stiffness matrix" which is consistent with this statement. If this is appended to the weighted residual formulation of equation (16) with a large multiplier λ, it forces

the weighted residual formulation to have a solution constrained by equation (24). The modified weighted residual statement is written as

$$\iiint_V \{\nabla W \cdot (\rho_r \nabla \phi + \rho \nabla \phi_r) - \mathrm{i}\eta_r W \rho\} \, \mathrm{d}V = \mathrm{i}\eta_r \iint_{S_s} W(\rho_{r_l} - \rho_{r_u})\zeta \, \mathrm{d}S + \iint_S W(\rho_r \nabla \phi + \rho \nabla \phi_r) \cdot \mathbf{n} \, \mathrm{d}S - \lambda \iint_{S_s} \bar{W} \Delta p \, \mathrm{d}S. \tag{30}$$

The weighting functions $\bar{W}(x)$ introduced in equation (30) are the pressure difference interpolation functions identified in equation (28). The penalty integral, equation (29), is introduced along the shear layer and produces penalty stiffness matrices which bridge the shear layer and include nodal values of acoustic potential on both sides of the shear layer. This is most easily implemented in the finite element context by introducing transition or bridging elements on the shear layer as shown in Figure 6. These elements are of zero thickness with three nodes on the top and three on the bottom to connect to the three nodes on the conventional triangular or quadrilateral elements above and below the shear layer. Finite element assembly proceeds as with other elements in the mesh. No new global nodes are introduced and there is no change in the bandwidth of the formulation nor to the sequence of operations in the equation solving procedure.

The boundary integral on S represents natural boundary conditions which must be imposed on the other boundaries of the domain. The far field boundary C_∞ is at a large distance from the nacelle and is a non-reflecting surface on which a radiation condition is applied via the boundary integral. This surface is the outer boundary of wave envelope elements which allow a transition from a fine mesh near the nacelle to a very coarse mesh in the far field. Most of the nacelle and centre body surfaces are rigid, where the normal component of acoustic particle velocity vanishes. In addition, the normal component of the mean flow velocity also vanishes and the flow tangency condition requires that $\nabla \phi_r \cdot \bar{n} = 0$, eliminating the boundary integral. A portion of the fan duct and centre body is acoustically treated. On these surfaces an impedance relation is specified, and this can be introduced through the boundary integral. The acoustic source is also introduced using the boundary integral. Details of the imposition of natural boundary conditions can be found in references [1–4].

In the results presented here there is no difference in steady flow density across the shear layer. The boundary integral on S_s which arises from considerations of conservation of acoustic particle displacement across the shear layer therefore vanishes.

8. ACOUSTIC TREATMENT ON DUCT WALLS

In the FEM formulation described here provision has been made for acoustic treatment on the duct wall and on the centre body. In the present context the acoustic field is described in terms of an acoustic potential formulation, while the boundary condition relates pressure and particle velocity. The implementation is described in this section.

A locally reacting acoustic lining material specified by its frequency dependent impedance or admittance is placed on an interior surface of the duct. The boundary integral of equation (30) is the mechanism by which the boundary condition imposed by

this acoustic treatment is introduced. On surfaces where acoustic treatment is present the normal component of mean flow velocity vanishes and the lining boundary integral simplifies to

$$I_L = \iint_{S_L} W\rho_r \nabla\phi \cdot \mathbf{n}\, \mathrm{d}S, \tag{31}$$

where $\mathbf{v} \cdot \mathbf{n} = \nabla\phi \cdot \mathbf{n}$ is the normal component of acoustic particle velocity, $\mathbf{v}$. The unit normal $\mathbf{n}$ is directed out of the computational domain and therefore into the acoustic treatment. The acoustic treatment is described by a local impedance relationship which connects acoustic pressure to a conceptual wall displacement velocity. In general, the types of acoustic treatment of interest are porous and the wall intself does not displace but the fluid in the pores does. It is the fluid velocity in the porous wall, directed normal to the wall, which is referred to as wall displacement velocity. The impedance relationship is of the form

$$\frac{p}{v_n} = Z = \frac{1}{A}, \tag{32}$$

where p is the non-dimensional acoustic pressure and v_n is the non-dimensional wall displacement velocity, directed into the wall. The impedance Z is a prescribed function of frequency and is non-dimensional with respect to $\rho_\infty c_\infty$, that is, the dimensional impedance would be $\rho_\infty c_\infty Z$. A is defined as the non-dimensional acoustic admittance. The relation between the fluid particle velocity at the wall and the wall velocity is one of continuity of particle displacement. This yields

$$\mathbf{v} \cdot \mathbf{n} = \pm\left(\frac{\partial\zeta}{\partial t} + M_w \frac{\partial\zeta}{\partial x}\right), \tag{33}$$

where $\zeta(x, \theta, t) = \zeta(x)\, \mathrm{e}^{\mathrm{i}(\eta_r t - m\theta)}$ is the wall displacement normal to the wall mean position, positive directed into the wall, and related to v_n by $v_n = \partial\zeta/\partial t$. M_w is the steady flow velocity at the wall, non-dimensional with respect to c_∞. The choice of positive or negative sign depends on whether the acoustic treatment is on the outer or inner wall of an annular duct. It is assumed that all lined surfaces have negligible curvature in the direction of the duct axis so that the rigorous description of the flow/surface kinematics [6] is simplified. With harmonic time dependence,

$$\mathbf{v} \cdot \mathbf{n} = \frac{1}{\mathrm{i}\eta_r}\left(\mathrm{i}\eta_r + M_w \frac{\partial}{\partial x}\right) v_n. \tag{34}$$

The relation between acoustic particle velocity and acoustic pressure is

$$\mathbf{v} \cdot \mathbf{n} = \pm\left(\mathrm{i}\eta_r + M_w \frac{\partial}{\partial x}\right) Ap. \tag{35}$$

The relation between acoustic pressure and acoustic velocity potential is provided by the acoustic Bernoulli equation of equation (19). Equation (35) can be rewritten

$$\mathbf{v} \cdot \mathbf{n} = \mp\frac{1}{\mathrm{i}\eta_r}\left(\mathrm{i}\eta_r + M_w \frac{\partial}{\partial x}\right)\left[\rho_r A\left(\mathrm{i}\eta_r + M_w \frac{\partial}{\partial x}\right)\phi\right]. \tag{36}$$

The boundary integral becomes

$$\mp \iint_{S_L} \rho_r W \mathbf{v} \cdot \mathbf{n} \, \mathrm{d}S = \mathrm{i}\eta_r \iint_{S_L} WA\rho_r^2 \phi \, \mathrm{d}S + \iint_{S_L} WA\rho_r^2 M_w \frac{\partial \phi}{\partial x} \, \mathrm{d}S$$

$$+ \iint_{S_L} W\rho_r M_w \frac{\partial}{\partial x} [A\rho_r \phi] \, \mathrm{d}S - \frac{\mathrm{i}}{\eta_r} \iint_{S_L} W\rho_r M_r \frac{\partial}{\partial x} \left[A\rho_r M_w \frac{\partial \phi}{\partial x} \right] \mathrm{d}S. \tag{37}$$

The upper and lower sign choice depends on whether the outer or inner wall integral is considered. The first two integrals on a boundary where acoustic treatment is present are easy to implement in the finite element formulation because only continuity of acoustic potential is required. The admittance, A, is assumed piecewise continuous and non-zero on a portion of the interior surface of the duct. An integration by parts, which is essentially an application of Stokes' Theorem on the interior surface, is performed to make the last two integrals compatible with the weak formulation. The integral representing the boundary condition on interior surfaces can now be written

$$\mp \iint_{S_L} \rho_r W \mathbf{v} \cdot \mathbf{n} \, \mathrm{d}S = \mathrm{i}\eta_r \iint_{S_L} WA\rho_r^2 \phi \, \mathrm{d}S + \iint_{S_L} WA\rho_r^2 M_w \frac{\partial \phi}{\partial x} \, \mathrm{d}S$$

$$- \iint_{S_L} (A\rho_r \phi) \frac{\partial}{\partial x} (W\rho_r M_w) \, \mathrm{d}S + \frac{\mathrm{i}}{\eta_r} \iint_{S_L} \left(A\rho_r M_w \frac{\partial \phi}{\partial x} \right) \frac{\partial}{\partial x} (W\rho_r M_w) \, \mathrm{d}S. \tag{38}$$

Equation (38) is in a form which is appropriate for application of standard finite element techniques to generate "boundary matrices" which are appended to the element stiffness matrices of elements whose outer boundaries represent acoustically treated surfaces.

9. AN ABSORBING BAFFLE

A restriction of the present FEM mesh is the presence of the baffle which is used to limit the computational domain, presumably with little reduction in the quality of the solution. It is assumed that the baffle is swept back at least 90° from the angle of peak radiation, however, this condition is often violated because it requires a mesh generation change to accomplish it. In theory the baffle is non-reflecting at large distances from the nacelle since it is a ray extending from the origin [2]. Near the intersection of the baffle and the nacelle the baffle is a reflecting surface and its presence has the possibility of contaminating the solution with spurious reflections. Experience has shown that the baffle has little effect on the peak lobe in the radiation pattern if the 90° rule is adhered to. However, there has been interest in using the inlet code and aft radiation code to generate the SPL directivity on the full 180° arc around the engine. This would be accomplished by separately obtaining the inlet and aft radiation results and then superposing them. Presumably, the peak lobes fore and aft would be little affected but the region at 90° to the engine axis would be critically dependent on a legitimate superposition of the inlet and aft results. This is not possible to achieve because of the baffle, unless it is completely non-reflecting.

An investigation has been made of the possibility of making the baffle at least partially non-reflecting. This has been done by introducing absorption on the baffle. As in the case of the nacelle acoustic treatment, this is done through the surface integral on S in

equation (30). On the baffle it is assumed that the flow is adequately represented by the uniform Mach number $\mathbf{M}_\infty = M_\infty \mathbf{i}$. This is true far from the nacelle, and is approximately true near the nacelle. The acoustic density perturbation is given by equation (17) evaluated with $\rho_r = 1$ and $c_r = 1$, assuming that far field steady flow conditions apply on the baffle. The surface integral on the baffle can then be written as

$$\iint_{S_b} W(\rho_r \nabla\phi + \rho \nabla\phi_r) \cdot \mathbf{n}\, \mathrm{d}S = \iint_{S_b} W\left[\nabla\phi \cdot \mathbf{n} - (\mathbf{M}_\infty \cdot \mathbf{n})\left(\frac{\partial\phi}{\partial t} + \mathbf{M}_\infty \cdot \nabla\phi\right)\right] \mathrm{d}S, \quad (39)$$

where $\mathbf{n}$ is the unit normal of the computational domain. The impedance condition on the baffle surface is defined simply as

$$p = \frac{Z_b}{\rho_\infty c_\infty} \mathbf{v} \cdot \mathbf{n}. \quad (40)$$

$Z_b/\rho_\infty c_\infty$ is the non-dimensional impedance and $Z_b/\rho_\infty c_\infty = 1/A$, where A is the non-dimensional admittance. This impedance condition corresponds to no real physical situation but rather is introduced to provide absorption on a notional boundary through which there is a steady mean flow. The acoustic Bernoulli equation (19) and the definition of the acoustic velocity potential

$$\mathbf{v} = \nabla\phi \quad (41)$$

leads to the conclusion that on the baffle,

$$\nabla\phi \cdot \mathbf{n} = -\frac{\rho_\infty c_\infty}{Z_b}\left(\frac{\partial\phi}{\partial t} + \mathbf{M}_\infty \cdot \nabla\phi\right). \quad (42)$$

The boundary integral can therefore be written as

$$\iint_{S_b} W(\rho_r \nabla\phi + \rho \nabla\phi_r) \cdot \mathbf{n}\, \mathrm{d}S = -\iint_{S_b} W\left[\left(\frac{\rho_\infty c_\infty}{Z_b} + \mathbf{M}_\infty \cdot \mathbf{n}\right)\left(\frac{\partial\phi}{\partial t} + \mathbf{M}_\infty \cdot \nabla\phi\right)\right] \mathrm{d}S. \quad (43)$$

The boundary integral of equation (43) is applied only in the near field portion of the baffle. In the wave envelope region the theoretically non-reflecting character of the far field baffle is left unchanged. The introduction of a locally reacting impedance boundary on the baffle cannot be expected to produce complete absorption any more than on the wall of a duct. As will be shown, only a modest absorption can be achieved.

10. POSTPROCESSING

Postprocessing of the acoustic velocity potential solution using the acoustic Bernoulli equation (19) to obtain acoustic pressure can be carried out in two ways. The approach which is most efficient computes acoustic pressure at the element nodes using the element shape functions. The nodal values are then averaged, to account for the fact that derivatives of potential are not continuous across element boundaries in the FEM formulation. For sufficiently fine meshes this produces acceptable results. Results presented in this paper are obtained by this method.

A second method available for postprocessing acoustic velocity potential to obtain acoustic pressure carries out the calculations at Gauss points in each element. The Gauss

points are known to be points at which optimal accuracy is achieved in the calculation of derivatives and therefore in calculation of acoustic pressure. The number of Gauss points is generally less than the number used in the Gauss integration in the formulation of the element stiffness matrices. The array of solution points on the grid constructed in this way can then be plotted as contours of equal acoustic pressure or equal sound pressure level using one of several available commercial plotting packages.

11. SOLUTION TECHNIQUES

The principal advantage of the FEM formulation described here is that it is computationally relatively efficient and therefore provides a useful tool for design calculations. This efficiency decreases as the non-dimensional frequency of the acoustic source increases, requiring a proportional increase in the mesh density and a disproportionate increase in computation time (by approximately the square of the ratio in mesh density). For this reason it is appropriate to give some observations on the linear equation solving routine which accounts for almost the entire computational time.

Previous fan noise radiation codes [1–4] used a frontal solver due to Irons [8]. This was extremely efficient in the use of active memory, partly because of considerable data transfer using direct access I/O in storing and retrieving element stiffness matrices in the assembly/solution procedure and in retrieving mesh and steady flow data. The resulting direct access files were subsequently read many times in the various FEM operations and in postprocessing. This efficiency in storage was offset by a significant cost in execution time. Nacelle design and source modelling have become the primary uses of the codes and execution time is a primary issue in a work station environment in which storage has become a much less limiting factor. Direct access operations are efficient from a programming standpoint, but inefficient in I/O time. In the version of the radiation code reported here all direct access I/O has been eliminated in favour of active storage or sequential I/O. This has resulted in as much as 50% reduction in computation time, dependent mainly on available fast memory.

Experiments with several popular iterative solution routines show that for the two-dimensional structure of problems considered here the direct solvers are always faster. This is consistent with the experience of other investigators [9]. There are indications that iterative solvers can be faster for similar problems in a three-dimensional geometry. The choice has been made to retain the modified Irons frontal solver.

12. EXAMPLE CALCULATIONS

The example calculations shown here are obtained on a mesh with about 27 000 degrees of freedom which is shown in Figures 4 and 5. This mesh becomes inadequate for non-dimensional frequencies much in excess of $\eta_r = 25$, and with the element distribution shown does better for acoustic radiation toward the sideline (high angular mode number or high radial mode number). Angular mode order corresponds to the value of m in the angular Fourier component $e^{-im\theta}$. Radial modes for a specified angular mode are enumerated beginning with $n = 1$. The geometry of the aft fan duct is generic, including an extended centre body and thin fan duct lip, in this case reflexed. The exterior Mach number is $M_o = 0{\cdot}2$ and the jet Mach number at the source plane is $M_j = 0{\cdot}5$.

The first result shows the success of the penalty method in implementing the condition of continuity of acoustic pressure across the shear layer. This is most effectively shown at low frequency because the acoustic field is relatively simple and the discontinuity in acoustic potential and continuity in acoustic pressure is easy to see. The frequency chosen

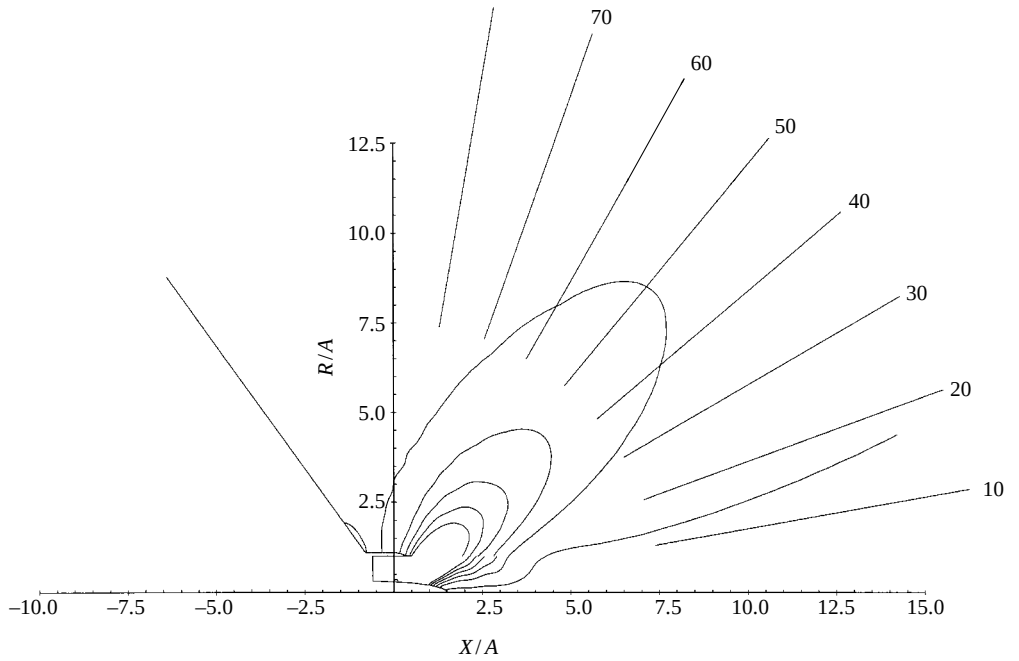

Figure 8. Contours of equal acoustic potential with $M_j = 0{\cdot}5$, $M_0 = 0{\cdot}2$. Reduced frequency $\eta_r = 5{\cdot}0$, input angular mode $m = 2$, radial mode $n = 1$, no acoustic treatment. Acoustic potential is discontinuous across the shear layer.

is $\eta_r = 5$ with an angular mode $m = 2$ and radial mode $n = 1$ input with unit pressure amplitude. The mesh is quite adequate for this low frequency. Figure 8 shows the radiated field in terms of contours of constant acoustic potential magnitude superimposed on the computational domain. In this example only five contours are produced to simplify the plot. The contours range from 15 dB above the maximum level on the outer boundary to 15 dB below. In Figure 8 it is clearly seen that the acoustic potential is discontinuous across the shear layer. Figure 9 shows similar contours of acoustic pressure and these are seen to be continuous across the shear layer. The pressure has been obtained by post-processing the potential field by using equation (19) with FEM interpolation at the nodes. Pressures thus obtained are averaged at common nodes. It is important to note that nodes across the shear layer are not common and the pressure across the shear layer is not averaged. The effectiveness of the penalty method is demonstrated by this example, as is the quality of the solution at this low frequency. Figure 10 shows an additional method of presentation of the radiation directivity. This represents calculations of sound pressure level on a circular arc at a radius of 10 duct radii from the origin, normalized to 100 dB maximum. In this case it emphasizes how broad the principle lobe is near the peak.

The results of Figure 10 can be used to compare the peak radiation angle in the principal lobe in the far field to predictions obtained using ray theory. A code has been written which is based on the analysis of Rice and Saule [10] for estimation of the radiation directivity from an exhaust duct. It is based on an extended analysis since it considers annular ducts while the original work of Rice and Saule considered only circular ducts. Propagation angles in the duct are determined from a formal eigenvalue/eigenfunction analysis and the convection and refraction effects are included as in reference [10]. It is predicted that the group velocity in the duct at the specified frequency and in the specified mode, $\eta_r = 5$, $m = 2$, $n = 1$, is at $34{\cdot}7^\circ$, and the phase velocity is at 51.2°. The peak propagation angle

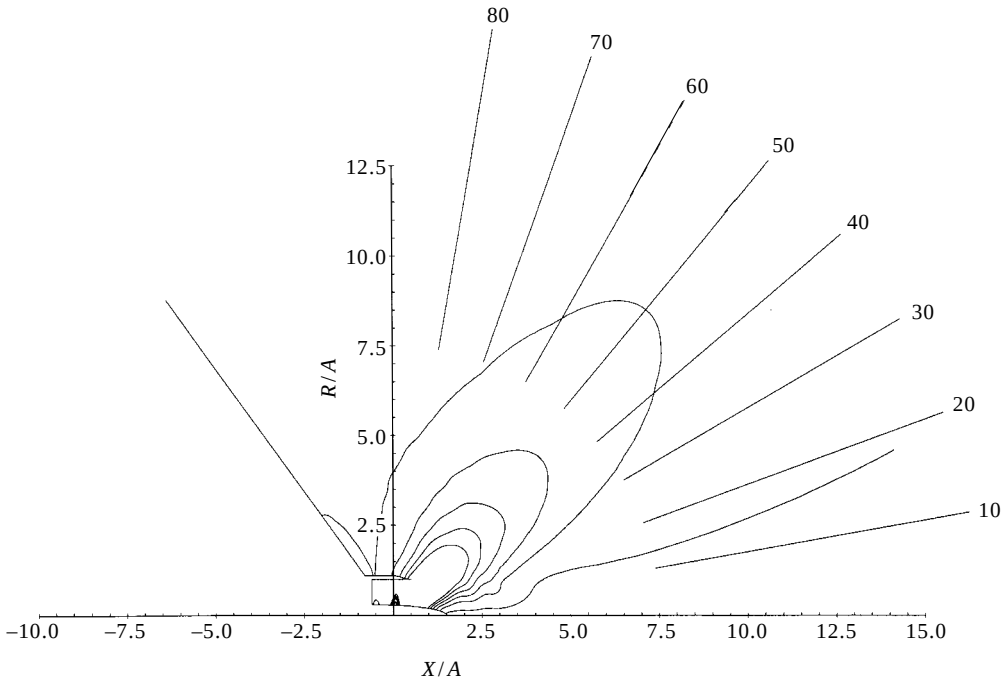

Figure 9. Contours of equal acoustic pressure with $M_j = 0{\cdot}5$, $M_0 = 0{\cdot}2$. Reduced frequency $\eta_r = 5{\cdot}0$, input angular mode $m = 2$, radial mode $n = 1$, no acoustic treatment. Acoustic pressure is continuous across the shear layer.

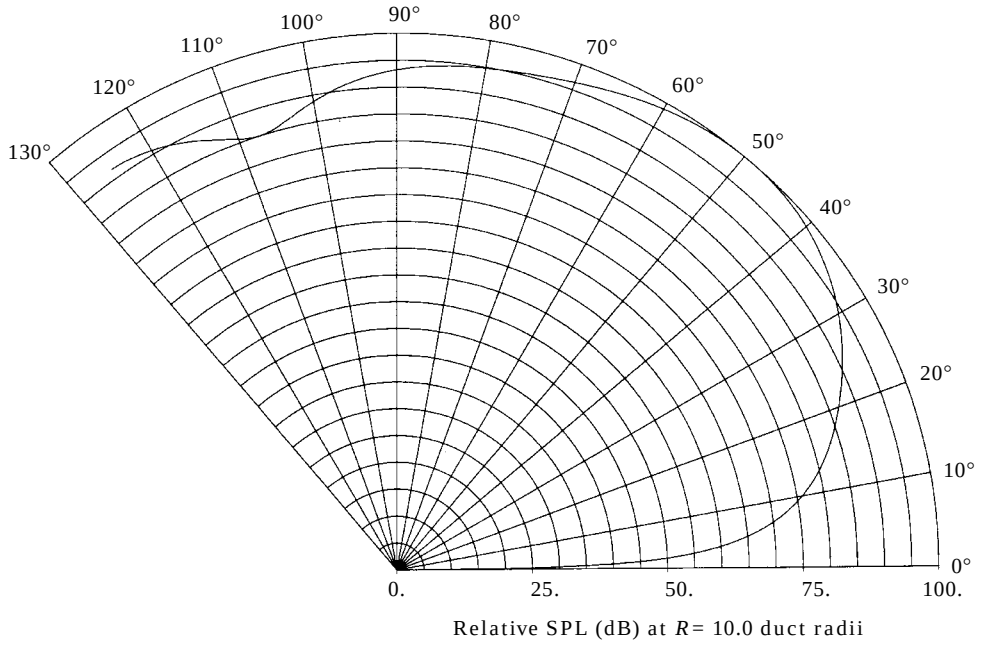

Figure 10. Radiation directivity on a circle of 10 duct radii centred on the computational origin. $M_j = 0{\cdot}50$, $M_0 = 0{\cdot}20$, $\eta_r = 5{\cdot}0$, $m = 2$, $n = 1$.

in the far field is estimated to be 49·5°. The observed angle of peak radiation in Figures 7 and 8 is around 50°, but the peak is so broad that it is difficult to pick the angle precisely. The correlation is excellent, although it must be pointed out that the mesh origin (0·5 duct radii back from the duct exit plane) is used in defining the directivity in this example. The Rice/Saule analysis would be based on an origin at the duct exit plane. Because the peak lobe is so broad there is little point in examining the effect of the origin shift on the stated comparison. This will be done in the next example which produces a sharper peak lobe.

A higher frequency case with a lower angle of peak radiation is the second example. In this case the non-dimensional frequency is $\eta_r = 25$ and the modal input is $m = 10$, $n = 1$. This is getting close to the limit of resolution for the mesh. Figures 11 and 12 show the two types of presentation for acoustic pressure. Figure 11 showing contours of constant SPL, while generally reasonably clean, emphasizes the assertion that the limit of resolution is close at hand. The breakdown of the mesh adequacy always appears in the near to intermediate field first and is usually related to mesh density in the region between the near field and the wave envelope region. The number of elements required in the generally radial direction is critical, and this can be minimized by bringing the wave envelope region in as close as possible. In the aft radiation case the jet interferes with this, and the wave envelope region must start far enough out that the jet is nearly entirely merged with the exterior flow. Figure 12 shows the polar directivity based on an origin at the exit plane (non-dimensional $x = 0{\cdot}5$) and demonstrates that these far field calculations are generally better than the near field because of the wave envelope interpolation. This mesh has been pushed to $\eta_r = 35$ without complete failure, and has the characteristic that it produces better results for modes which radiate well to the sideline than for those which radiate at relatively small angles to the axis as in these examples. This probably results from the complicated interaction of transmission and reflection of modes at near grazing incidence

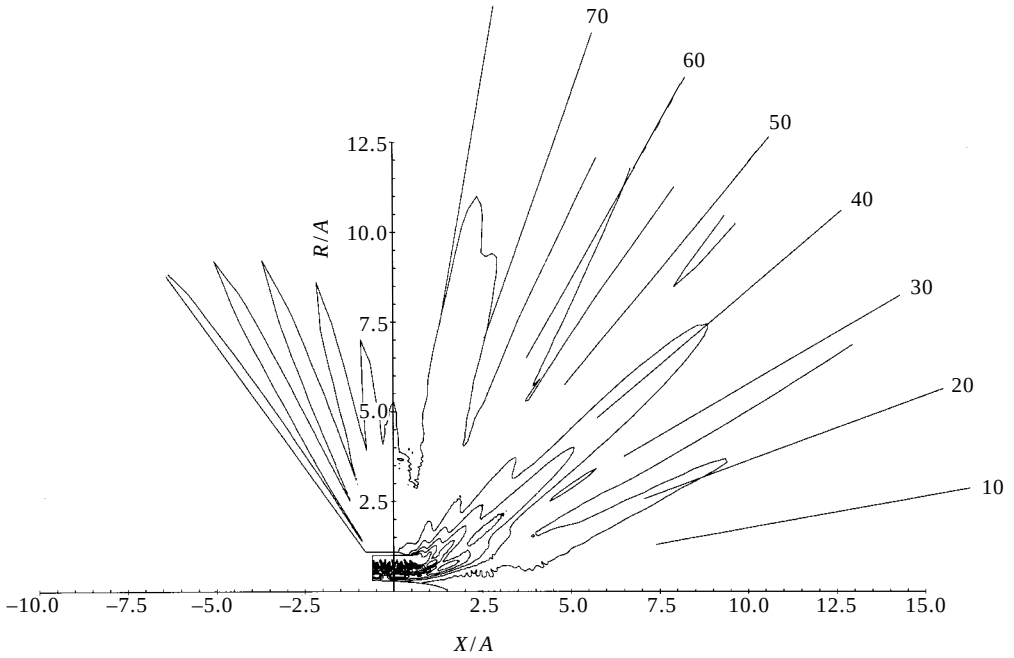

Figure 11. Contours of equal acoustic pressure with $M_j = 0{\cdot}5$, $M_0 = 0{\cdot}2$. Reduced frequency $\eta_r = 25{\cdot}0$, input angular mode $m = 10$, radial mode $n = 1$, no acoustic treatment. Acoustic pressure is continuous across the shear layer.

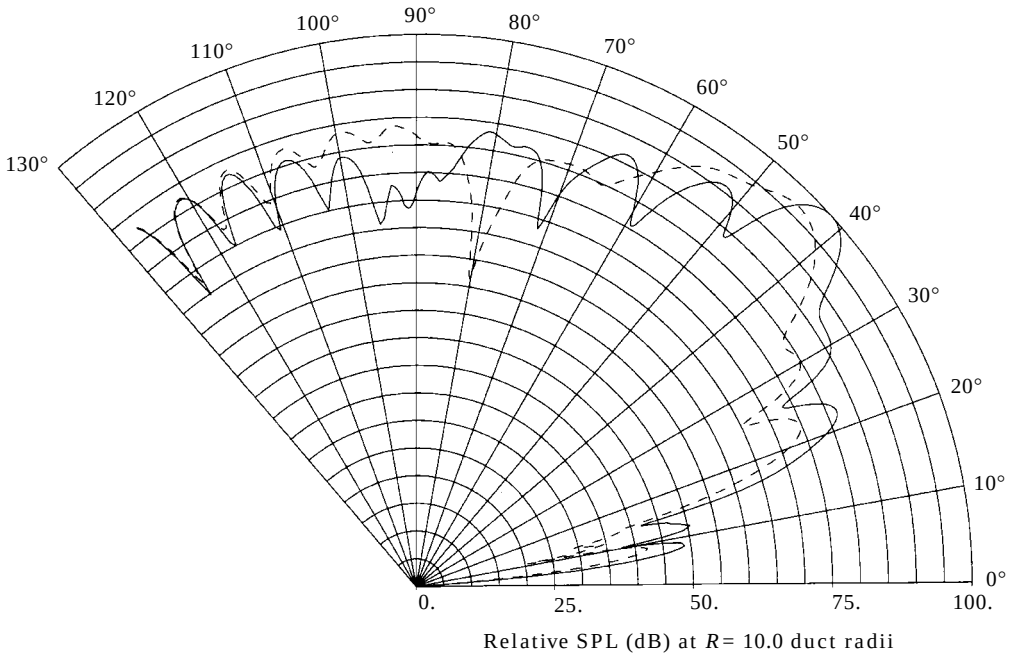

Figure 12. Radiation directivity on a circle of 10 duct radii centred on an origin at the fan duct exit plane, $x = 0{\cdot}5$, $M_j = 0{\cdot}50$, $M_0 = 0{\cdot}20$, $\eta_r = 25{\cdot}0$, $m = 10$, $n = 1$. ——, Case with no acoustic treatment; – – –, acoustically treated case with non-dimensional admittance $A = 0{\cdot}811 + i0{\cdot}081$.

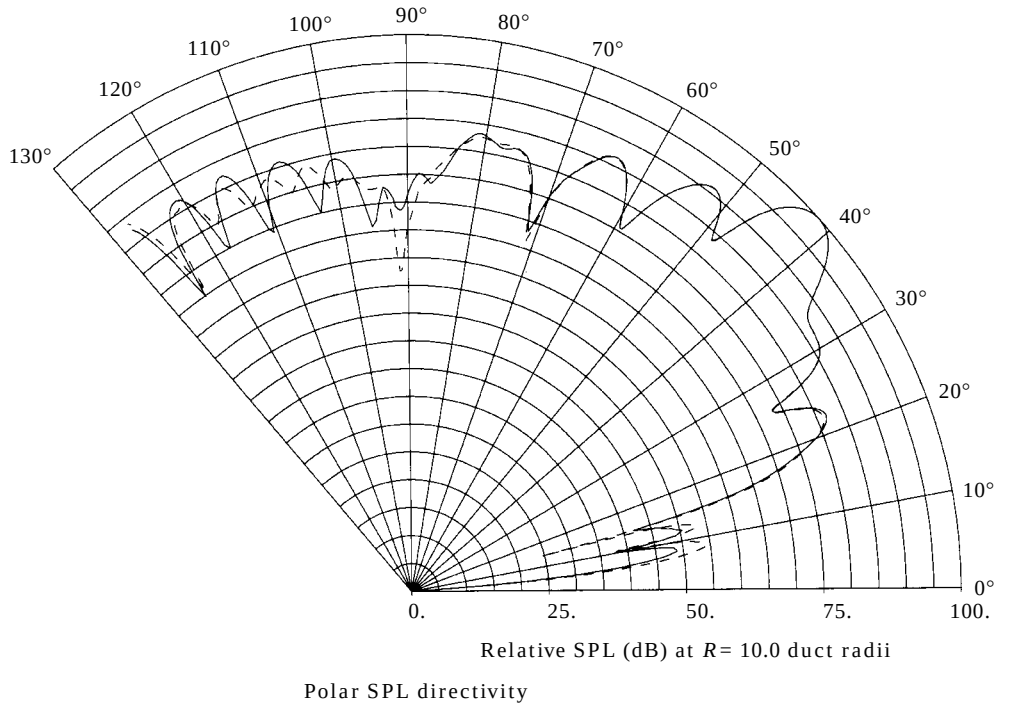

Figure 13. Radiation directivity on a circle of 10 duct radii centred on an origin at the fan duct exit plane, $x = 0{\cdot}5$, $M_j = 0{\cdot}50$, $M_0 = 0{\cdot}20$, $\eta_r = 25{\cdot}0$, $m = 10$, $n = 1$, no acoustic treatment in the duct. ——, Case with the baffle untreated; – – –, case with an absorbing boundary on the baffle in the near field.

at the shear layer. The mesh shown in Figures 4 and 5 has proven to be a good generic structure to work with.

Figure 12 can be used to compare the peak radiation angle in the principal lobe in the far field to predictions obtained using ray theory. It is predicted that the group velocity in the duct at the specified frequency and in the specified mode, $\eta_r = 25$, $m = 10$, $n = 1$, is at 27·4°, and the phase velocity is at 39·4°. The peak propagation angle in the far field is estimated to be 43·9°. The observed angle of peak radiation in Figure 12 is around 42° and is adjusted for the origin shift to the exit plane. The correlation with the Rice/Saule result is good, particularly when it is noted that flow conditions along the shear layer in the FEM calculations are not uniform, and within the jet region the Mach number is reduced below $M_j = 0{\cdot}5$ due to the gradual reduction in radius of the centre body. The effect can be observed if an average Mach number $M_j = 0{\cdot}45$ in the jet is used in the Rice/Saule approximation. The ray prediction would yield 41·9° which is about the same as the FEM prediction which accounts for the non-uniform Mach number in the jet.

An example of the effect of acoustic treatment on the duct walls is also shown in Figure 12. A locally reacting lining with normalized impedance and admittance given by $Z = 1{\cdot}221 - \mathrm{i}0{\cdot}122$, $A = 0{\cdot}811 + \mathrm{i}0{\cdot}081$ is assumed in the high frequency case. The impedance/admittance is optimum for the $\eta_r = 25$, $M_j = 0{\cdot}5$, $m = 10$, $n = 1$ mode. The outer wall of the fan exhaust duct and the centre body are lined over a length of 0·916 R beginning at 0·074 R forward of the assumed source plane. The attenuated directivity shown in Figure 12 reveals an attenuation of as much as 5 or 6 dB at polar angles below the shifted principal lobe which is now at about 45°. What was once a relatively well-defined principal lobe is now considerably broadened and beyond 45° there are areas in which the SPL is increased, primarily due to filling in of interference notches. The angle shift of the principal lobe is consistent with the fact that the effect of the acoustic treatment would be to increase the angle of the phase velocity and group velocity vectors (lower the cut-off ratio) within the duct.

Finally, Figure 13 is used to show the effect of an attempt to reduce the effects of reflection from the baffle. A resistive "lining" with non-dimensional admittance $A = 0{\cdot}8 + \mathrm{i}0{\cdot}0$ has been placed on the baffle in the region of conventional elements (the wave envelope elements in theory should not produce reflections). It is seen that there is an observable change in SPL at large polar angles (near the baffle) and in the region near the exhaust axis where the directly radiated field is at low SPL. Since it is not known what the true reflection free directivity should look like, no conclusion can be drawn other than the baffle does have an effect on the directivity at large angles, and that the effect is modestly changed when the baffle is made dissipative. Perhaps of more importance is the fact that virtually no effect is observed near the principal lobe, suggesting that the baffle has correctly been assumed to be non-intrusive in this region.

While not entirely definitive, the results shown here suggest that the FEM model of aft fan radiation captures the known refraction effects of the shear layer very well. Extensive bench marking of the code against experiments has been carried out by other investigators [11, 12]. Comparisons of calculations and measurements have been very good.

13. CONCLUSION

A finite element model for acoustic propagation and radiation within and exterior to the aft fan duct of a high by-pass turbofan engine has been developed. It is based on the assumption of irrotational acoustic perturbations on an irrotational steady flow. The jet is modelled in the steady flow calculations by a potential flow constrained by a shear layer and allowed to merge with the surrounding flow downstream of the fan duct exit plane.

The formulation is restricted to axisymmetric geometries and harmonic sources described by their angular and radial modal content. The condition of acoustic particle displacement continuity across the shear layer is shown to be satisfied by proper interpretation of a boundary integral which occurs in the FEM formulation. Continuity of acoustic pressure is implemented by introducing a penalty method based on the relationship between acoustic pressure and velocity potential. Example calculations have shown that the continuity of pressure is accurately enforced. Resolution of accurate solutions at high non-dimensional frequencies is limited by mesh density which has implications on storage requirements and execution time. In the present study computations with over 27 000 degrees of freedom have been shown to produce reasonable results up to the reduced frequency $\eta_r = 25$. Doubling the frequency would require an approximate doubling of the density of the mesh.

REFERENCES

1. J. S. Preisser, R. J. Silcox, W. Eversman and A. V. Parrett 1985 *Journal of Aircraft* **22**, 57–62. Flight study of induced turbofan inlet acoustic radiation with theoretical comparisons.
2. W. Eversman, A. V. Parrett, J. S. Preisser and R. J. Silcox 1985 *ASME Journal of Vibration Acoustics, Stress, and Reliability in Design* **107**, 216–223. Contributions to the finite element solution of the fan noise radiation problem.
3. A. V. Parrett and W. Eversman 1986 *AIAA Journal* **24**, 753–760. Wave envelope and finite element approximations for turbofan noise radiation in flight.
4. I. Danda Roy and W. Eversman 1995 *ASME Journal of Vibration and Acoustics* **117**, 109–115. Improved finite element modeling of the turbofan engine inlet radiation problem.
5. K. Karamcheti 1966 *Principles of Ideal Fluid Aerodynamics*. New York: Wiley. See pp. 190–194, 210–220.
6. M. K. Myers 1980 *Journal of Sound and Vibration* **71**, 429–434. On the acoustic boundary condition in the presence of flow.
7. T. J. R. Hughes 1987 *The Finite Element Method, Linear Static and Dynamic Finite Element Analysis*. Englewood Cliffs, NJ: Prentice-Hall. See pp. 185–303.
8. B. M. Irons 1970 *International Journal for Numerical Methods in Engineering* **2**, 5–32. A frontal solution program for finite element analysis.
9. B. Regan 1996 *PhD Dissertation, University College Galway, Ireland*. Development of finite element techniques for aeroacoustic applications.
10. E. J. Rice and A. V. Saule 1980 *NASA TM* 81506. Far field radiation of aft turbofan noise.
11. L. A. Heidelberg, D. L. Sutliff and M. Nallasamy 1997 *AIAA Paper AIAA*-97-1587, *Presented at the* 35*th Aerospace Sciences Meeting, Reno, NV*. Azimuthal directivity of fan tones containing multiple modes.
12. D. A. Topol 1997 *AIAA Paper AIAA*-97-1611, *Presented at* 3*rd AIAA/CEAS Aeroacoustics Conference, Atlanta, GA*. Development and evaluation of a coupled fan noise design system.